Raya Mertens[1]
Division of Production Engineering,
Machine Design and Automation,
Department of Mechanical Engineering,
University of Leuven (KU Leuven),
Leuven 3001, Belgium
e-mail: raya.mertens@kuleuven.be

Stijn Clijsters
Division of Production Engineering,
Machine Design and Automation,
Department of Mechanical Engineering,
University of Leuven (KU Leuven),
Leuven 3001, Belgium
e-mail: stijn.clijsters@kuleuven.be

Karolien Kempen
Division of Production Engineering,
Machine Design and Automation,
Department of Mechanical Engineering,
University of Leuven (KU Leuven),
Leuven 3001, Belgium
e-mail: karolien.kempen@kuleuven.be

Jean-Pierre Kruth
Division of Production Engineering,
Machine Design and Automation,
Department of Mechanical Engineering,
University of Leuven (KU Leuven),
Leuven 3001, Belgium
e-mail: jean-pierre.kruth@kuleuven.be

Optimization of Scan Strategies in Selective Laser Melting of Aluminum Parts With Downfacing Areas

Selective laser melting (SLM) is an additive manufacturing technique in which metal products are manufactured in a layer-by-layer manner. One of the main advantages of SLM is the large geometrical design freedom. Because of the layered build, parts with inner cavities can be produced. However, complex structures, such as downfacing areas, influence the process behavior significantly. The downfacing areas can be either horizontal or inclined structures. The first part of this work describes the process parameter optimization for noncomplex, upfacing structures to obtain relative densities above 99%. In the second part of this research, parameters are optimized for downfacing areas, both horizontal and inclined. The experimental results are compared to simulations of a thermal model, which calculates the melt pool dimensions based on the material properties (such as thermal conductivity) and process parameters (such as laser power and scan speed). The simulations show a great similarity between the thermal model and the actual process. [DOI: 10.1115/1.4028620]

Keywords: SLM, AlSi10Mg, downfacing structures

1 Introduction

SLM is a production technique that builds products in a layer-by-layer fashion. Figure 1 shows a schematic overview of the process. For each part-layer to be produced, a layer of powder, with a typical layer thickness of 30 μm, is deposited on the build platform. Subsequently, the laser scans predefined areas and melts the powder locally. Once the scanning is finished, the build platform moves down and the cycle repeats until the part is completed.

The use of different parameters determines the nature of the process. The scan strategy consists of two parts, namely, the scan parameters or parameter set (laser power, scan speed, scan spacing, and layer thickness) and the scan pattern (laser path).

The first requirement in the production of qualitative SLM parts consists of obtaining nearly fully dense parts [1,2]. To fulfill this requirement, the parameter set has to be optimized. This parameter set is used to produce parts without downfacing areas. Density optimization of aluminum is investigated before in Refs. [3] and [4].

A second requirement arises when parts with downfacing areas are produced. Such downfacing areas are often encountered in complex products with, for example, internal cooling channels. These areas need an adapted scan strategy. In these areas, the laser scans on top of several layers of unmolten powder, which changes the melting behavior. Optimizing the downfacing scan strategy enables the production of qualitative complex parts, thus enlarging the geometrical freedom and the number of applications of the SLM process.

Scan strategy optimization for downfacing areas is previously investigated in Ref. [5] for horizontal structures and in Ref. [6] for inclined structures. This research uses a strategy that is based on Ref. [5] to be able to produce horizontal downfacing areas.

2 Procedure

2.1 Equipment. The SLM machine used in this research is an in-house built machine of KU Leuven—PMA. Table 1 summarizes the properties of the optical setup. All parts were built in an Ar atmosphere.

2.2 Material. In this research, the scan strategy is optimized for AlSi10Mg. This aluminum alloy is a casting-alloy. Previous research [3,4] shows that AlSi10Mg is an alloy that is suitable for SLM, due to its high amount of silicon that improves the alloy's "fluid life."

The chemical composition of this alloy is presented in Table 2. The two most important alloying elements are silicon and magnesium. Silicon has limited solubility and yet undergoes a relatively large volume fraction of isothermal solidification, thus gaining significant strength while undergoing little or no thermal

Table 1 Laser properties of the in-house built SLM machine

Type	Yb fiber laser
Maximal power (P)	300 W
Wavelength (λ)	1064 nm
Spot diameter ($d_{99\%}$)	80 μm

[1]Corresponding author.

Contributed by the Manufacturing Engineering Division of ASME for publication in the Journal of Manufacturing Science and Engineering. Manuscript received April 15, 2014; final manuscript received September 9, 2014; published online October 24, 2014. Assoc. Editor: Darrell Wallace.

Table 2 Chemical composition of AlSi10Mg (ISO 3522)

	Al	Si	Fe	Cu	Mn	Mg	Zn	Ti	Others
Weight percentage	86.9–90.8	9.0–11.0	≤0.55	≤0.10	≤0.45	0.20–0.45	≤0.10	≤0.15	≤0.30

contraction. This is very important to avoid hot cracking issues. Magnesium's role is to strengthen and harden the aluminum alloy. Silicon combines with magnesium to form the hardening Mg_2Si phase.

2.3 Parameter Optimization. In the first step of this research, the scan parameters are optimized in terms of density. After this optimization, simple geometries with nearly full-density can be produced.

In a second step, downfacing structures (both horizontal and inclined) are considered. They require an adapted scan strategy to avoid dross formation or collapsing downfacing surfaces (Fig. 2).

2.3.1 Density Optimization for Cubic Parts. In order to produce fully dense parts, the scan parameters (laser power, scan speed, scan spacing, and layer thickness) have to be carefully optimized [7–9]. In this research, laser power and scan speed are varied, while the scan spacing and layer thickness are kept constant at, respectively, 105 μm and 30 μm. These parameters were determined in initial research on SLM of AlSi10Mg [3], and this research shows that they are also applicable here.

In the scan pattern that was used, the laser tracks within one layer are parallel but have alternating directions (zig–zag). This pattern is rotated over 90 deg for consecutive layers.

The relative density of the parts is measured by Archimedes' principle. The samples are weighted both in air and in ethanol. Based on the difference in weight and the density of ethanol, density values are calculated. Dividing these values by the theoretical value of the material results in relative density values. Besides Archimedes, optical microscope images are used to verify the size, morphology, and distribution of the pores.

2.3.2 Downfacing Structures. Downfacing structures need an adapted scan strategy. Because downfacing areas are scanned on multiple layers of loose powder (instead of on solidified material), their melt pool behavior is different. Due to the lower (and non-uniform) heat-conductivity of the powder, the melt pool becomes very unstable and deep if the scan strategy is not optimized, resulting in random dross formation (Fig. 2).

The parameter optimization is based on simulations of a thermal model and on experimental tests. The thermal model is developed within the University of Leuven (KU Leuven). The model is based on an enthalpy formulation [Eq. (1)], which is nonlinear due to the relation between temperature and enthalpy. Enthalpy values of the material are calculated numerically by using explicit forward Euler time integration and central differencing for the space derivatives. The aggregation states of the material are then obtained based on these enthalpy values [10].

The experimental tests focus on the density of the entire part and of the downfacing layers in particular, geometrical accuracy and surface quality. Evaluation is mainly based on microscope images and visual inspection

$$\frac{\partial H}{\partial t} = \nabla \cdot k\nabla T + S_V + S_S \tag{1}$$

where H is enthalpy, T is temperature, t is time, S_V is volume source term, k is thermal conductivity, and S_S is surface source term.

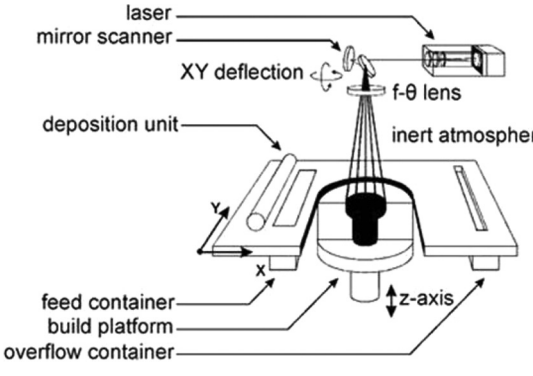

Fig. 1 Schematic overview of the SLM process

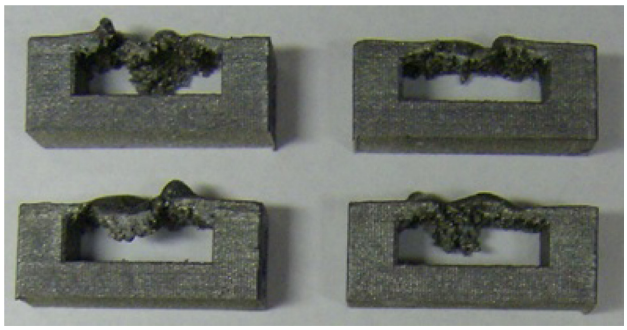

Fig. 2 Dross formation due to deep unstable melt pool in downfacing areas with a length of 10 mm

Figure 3(*a*) shows the geometry and dimensions of the produced parts, containing downfacing areas.

Besides horizontal downfacing structures, inclined structures are also taken under investigation (Fig. 3(*b*)). To check the angles of the produced parts, a vision measuring system (Quick Vision Pro 202) is used [11]. On these images, the upfacing and downfacing edges of the part cavity are fitted by lines through a minimum of 60 points and the angle between these two edge lines is measured.

3 Results and Discussion

3.1 Density Optimization for Cubic Parts. Figure 4 shows the relative densities achieved for each combination of laser power and scan speed. For aluminum alloys in general, the use of high powers results in high densities. Therefore, the power is varied between 240 W and 300 W, which is the maximum power of the laser. The scan speed is varied in a way that densities higher than 99% are achieved, without using scan speeds that are too low in order to guarantee the productivity of the process.

In this parameter range, densities increase when power increases or scan speed decreases. Hence, the density increases when the energy input increases. This energy input is presented by Eq. (2). Relative densities are higher than 99% when ϕ is larger than 0.2 Ws/mm.

$$\phi = \frac{P}{v} \tag{2}$$

The optimal parameter set in terms of part density consists of a laser power of 300 W and a scan speed of 1400 mm/s. A high power is preferable because it allows a higher scan speed and therefore a high productivity. The relative density based on five parts is 99.3%±0.2% (95% confidence interval).

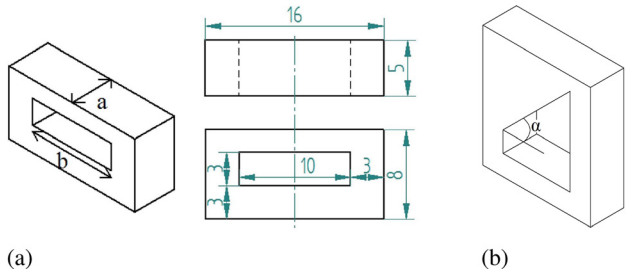

Fig. 3 Downfacing structures. (*a*) Horizontal and (*b*) Inclined.

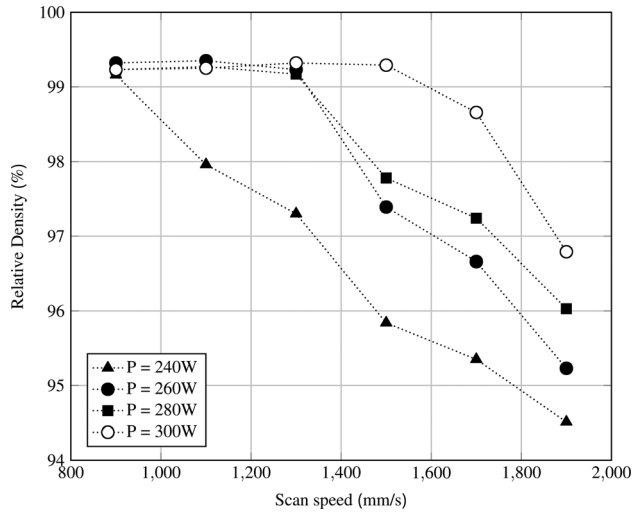

Fig. 4 Relative density in function of scan speed and laser power

These high densities are confirmed using light optical microscopy. Figure 5 shows a top view and a side view of an SLM-cube. There are still pores present in the workpiece, but they are very small, and the number of pores is limited. The pores are mainly situated near the borders of the piece.

3.2 Downfacing Structures. Research on downfacing structures is divided into three parts: horizontal downfacing structures, extended or large horizontal downfacing structures, and inclined structures.

3.2.1 Horizontal Downfacing Structures. Previous research on downfacing areas in Ti6Al4V [5] indicates the successful use of different parameter zones above the downfacing area (Fig. 6). This strategy is also used in this work.

The area above the downfacing surface is divided into five zones. These zones each consists of multiple layers and they all have an adapted parameter set. In this way, a gradual transition to the standard parameters (parameters to obtain optimal density) of 300 W and 1400 mm/s can be accomplished.

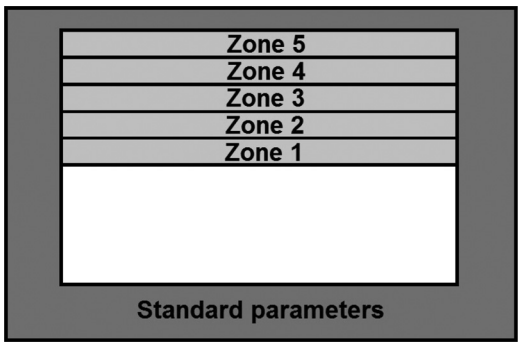

Fig. 6 Different zones of a downfacing structure

To find an optimal parameter set for the five adapted zones, first a parameter set for the first zone has to be estimated. Parameters for the following zones are obtained by making a smooth transition from zone 1 to standard parameters.

The optimal parameter set for the first downfacing zone is determined based on simulations on one side, and on experimental tests on the other side.

Two scanning parameters have to be optimized: laser power (P) and scan spacing (h). To guarantee an acceptable productivity, scan speed (v) is kept constant at 1400 mm/s.

Thermal model. Simulations are performed both for a normal scanning situation (Fig. 7(*a*)) and a downfacing scanning situation (Fig. 7(*b*)). In the normal scanning situation, the laser scans one layer of powder (represented by the top 30 μm in the figure) on top of a solid base. The melt pool is also visible in the simulation. This simulation uses a power of 300 W and scan speed of 1400 mm/s as was found to be the optimal parameter set for normal, upfacing scanning situations.

In the downfacing scanning situation (Fig. 7(*b*)), the downfacing geometry is simulated. The left pillar is shown between 0 and 120 μm along the x-axis. After 120 μm, the volume is filled with powder. Here, three different powers of 20 W, 60 W, and 300 W are used.

Because only single-tracks are simulated, no conclusions can be drawn about the scan spacing.

From Fig. 7(*b*), it is clear that the melt pool enlarges with increasing power. To insure a stable melt pool, the melt pool dimensions cannot be too small, nor too large in order to avoid irregularities or droplets [3]. The melt pool dimensions can be evaluated by comparing them to the melt pool dimensions of the normal scanning situation, because the experimental tests showed that this corresponds to a stable melting situation. Melt pool width and depth of the 60 W downfacing situation is similar to the dimensions of the normal scanning situation (width of 125 μm and depth of 60 μm). A power of 20 W results in a melt pool that is too small; a power of 300 W (which is used for the normal scanning situation) results in a very large melt pool. This is due to the lower heat

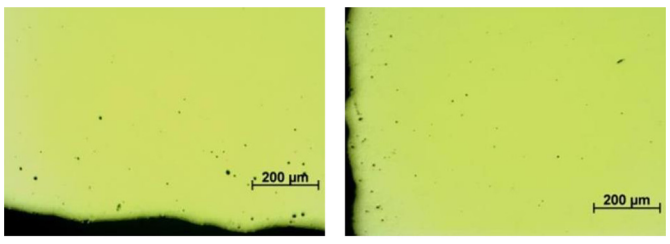

Fig. 5 Microscope images show high density of 99.3%. (*a*) Top view and (*b*) Side view.

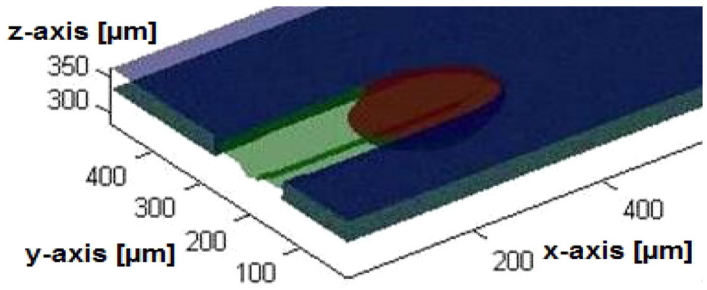

(a)

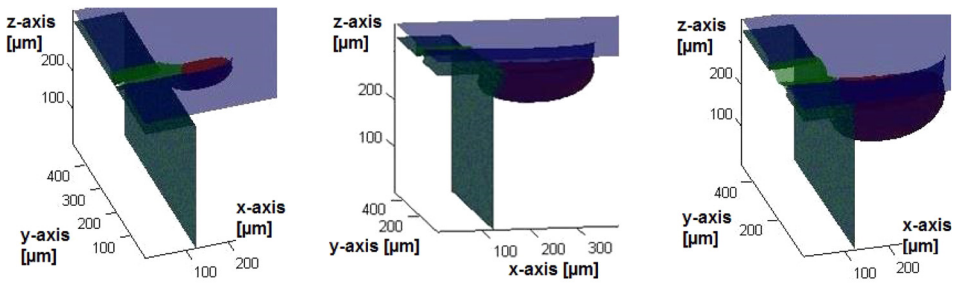

$P = 20W$ $P = 60W$ $P = 300W$

(b)

Fig. 7 Simulation results. (*a*) Normal scanning situation on solidified material and (*b*) Downfacing scanning situation.

conductivity of the powder material in comparison to solid material.

Based on the thermal model, a laser power of approximately 60 W results in a stable process.

Experimental tests. In these tests, first the effect of the scan spacing is investigated. Reducing the scan spacing results first in smoother surfaces until it reaches an optimal value. Further reducing the scan spacing then leads to rougher surfaces. An optimal scan spacing is found to be 20 μm.

To determine the optimal laser power, several parts with different laser powers of zone 1 are produced and compared. Figure 8 gives an overview. The power is varied between 40 W and 90 W. Outside of these values, the production fails due to curling up of the downfacing layers.

When the power of the first zone is too low, no powder is melted. On the other hand, when power is too high, large irregular lumps are formed. These lumps lower the surface quality and can cause problems in post-treatments like sandblasting or etching. These lumps are also visible to the naked eye. Figure 9 compares downfacing surfaces scanned with laser powers of 35 W and 85 W. In the image of 85 W, larger lumps are visible. The conclusion here is that there is a relative large range of applicable powers, but the results show large differences. A power of 60 W insures that in the first downfacing layers some powder is already molten while avoiding large lump formation.

Results. Both simulations and tests indicate a power of 60 W to be used for the first zone of the downfacing structure. According to the experimental tests, a scan spacing of 20 μm is recommended.

Now that the parameters for the first zone are determined, parameters for the next zones are obtained by making the smooth transition to standard parameters.

The optimal scan strategy for horizontal downfacing structures is displayed in Table 3. From this table, it is clear that the power increases every zone. Because of the increase in power, the scan spacing has to be larger for zone 2 in comparison to zone 1.

Every zone requires ten layers to obtain a stable process.

Figure 10 shows the produced downfacing structures.

Figure 11 shows a cross section that is taken perpendicular to the image of Fig. 10. It is clear that there is warp present toward the front and the back of the structure. The warp is a result of thermal stresses that are present in the SLM-pieces. On the borders of the downfacing structure, there is no mechanical support. This also implies that there is no heat sink present at these borders which complicates the heat dissipation. This results in curling only at these location. Figure 11 shows that the sides only have a thickness of about ten layers (300 μm) instead of the designed 60 layers (1800 μm).

3.2.2 Extended/Larger Downfacing Structures. When producing larger downfacing areas, results are influenced by the heat transport situation [12]. In a small downfacing area, the main direction in which heat is conducted points from the middle of the downfacing structure to the sides as shown in Fig. 12.

In wide downfacing structures (the width is presented by *a* in Fig. 3), this situation does not change. The path the heat has to travel still has the same length. That is why wide downfacing structures can easily be produced using the scan strategy from Table 3. Figure 13 demonstrates this. Here, a downfacing structure with a width of 40 mm is produced.

Problems however, arise when long downfacing structures are produced (the length is presented by *b* in Fig. 3). The path from the middle of the downfacing structure to the sides becomes longer and without extra measures, the downfacing structure will fail.

The geometry of Fig. 14(*a*) offers a solution for this problem. In this geometry, extra supports are placed at the edges of the downfacing structure. These supports provide extra channels for heat transport. They also give more mechanical support to the downfacing structure. The result of this geometry scanned with the strategy from Table 3 is displayed in Fig. 14(*b*).

3.2.3 Inclined Structures. Because of the less extreme situation, the adapted strategy for inclined downfacing structures is limited to only three zones before using standard parameters.

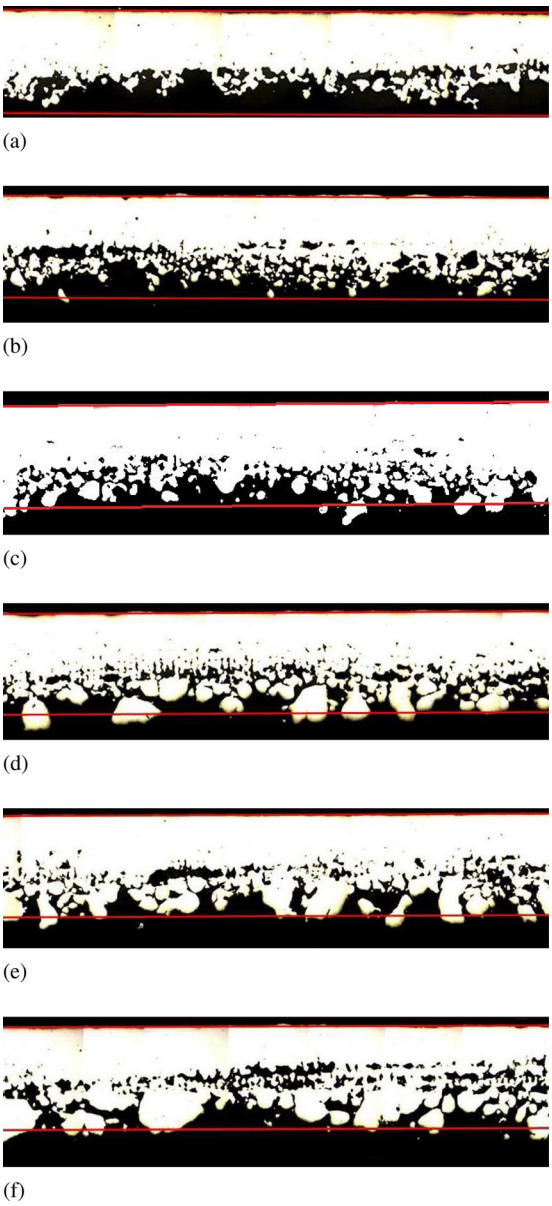

Fig. 8 Comparison of the different powers used in zone 1. The lines indicate the borders of a perfect downfacing area. The length of the pieces is 10 mm. (*a*) 40 W, (*b*) 50 W, (*c*) 60 W, (*d*) 70 W, (*e*) 80 W, and (*f*) 90 W.

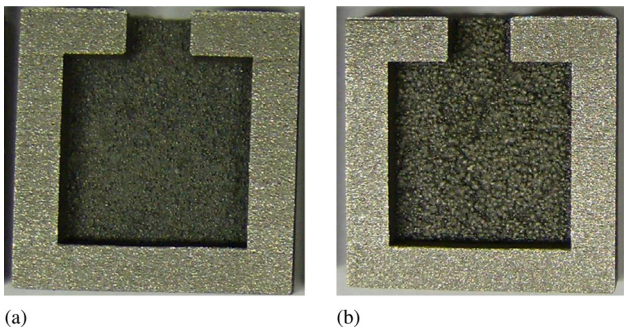

Fig. 9 Comparison of two downfacing areas of 14 mm × 14 mm. When using high powers, large lumps are formed. (*a*) 35 W and (*b*) 85 W.

Table 3 Optimal parameter set for downfacing structures in AlSi10Mg ($v = 1400$ mm/s)

	Z1	Z2	Z3	Z4	Z5	Standard parameters
Laser power (W)	60	90	120	150	220	300
Scan spacing (μm)	20	110	110	110	110	110
Number of layers	10	10	10	10	10	Rest (here 10)

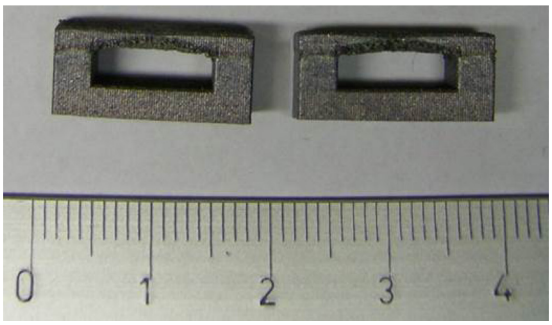

Fig. 10 Picture of a downfacing structure with a length of 10 mm

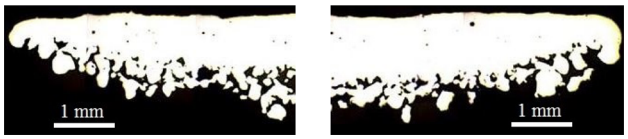

Fig. 11 Warp of the downfacing structure

Fig. 12 Heat transport situation in downfacing structures

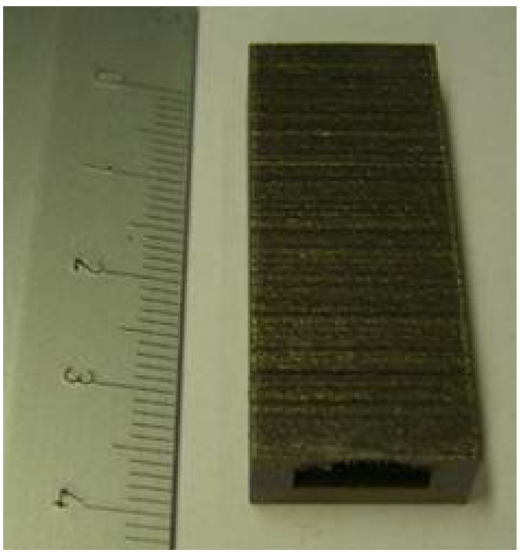

Fig. 13 Wide downfacing structure of 40 mm

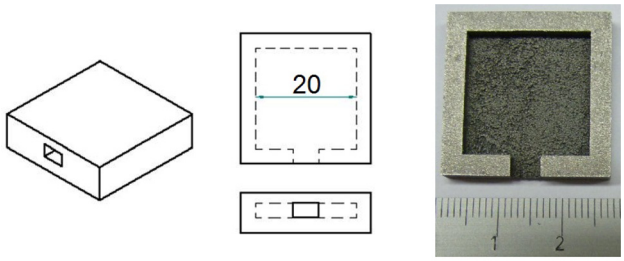

Fig. 14 Adapted geometry to obtain longer downfacing structures with a length of 20 mm. (*a*) Geometry and (*b*) Result.

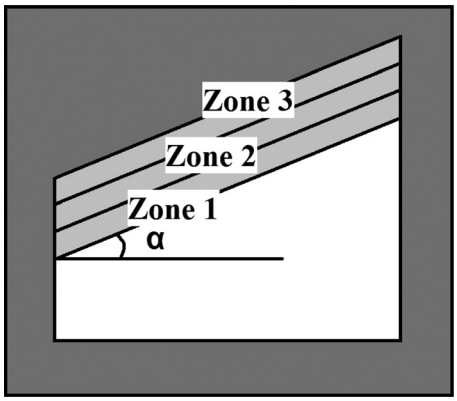

Fig. 15 Different zones of an inclined area with angle α

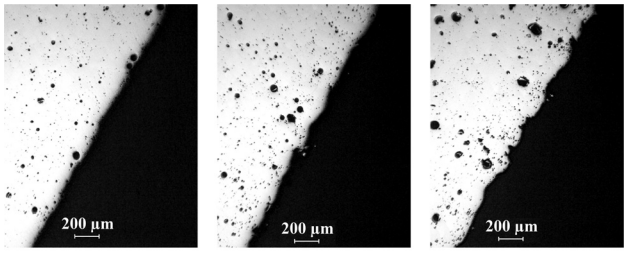

Fig. 16 Microscope images of inclined structures ($\alpha = 60$ deg) with different power used in zone 1. (*a*) 100 W, (*b*) 200 W, and (*c*) 300 W.

Fig. 17 Microscope images of inclined structures ($\alpha = 45$ deg) with different power used in zone 1. (*a*) 100 W, (*b*) 200 W, and (*c*) 300 W.

Table 4 Scan strategy for inclined structures with an angle of 30 deg

	Zone 1	Zone 2	Zone 3	Standard parameters
Power (W)	120	150	180	300
Number of layers	15	15	15	Rest

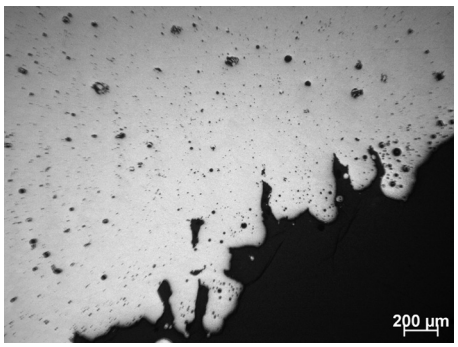

Fig. 18 Microscope image of the inclined structure of 30 deg

Figure 15 illustrates this strategy. In this strategy, each zone uses the same scan spacing of 110 μm. Parameters are optimized for three inclination angles, namely 60 deg, 45 deg, and 30 deg. These angles are defined as shown in Fig. 15.

Inclined angle of 60 deg. Structures with an inclined angle of 60 deg can be produced with a laser power of 300 W in all zones. The result of such a structure is shown in Fig. 18. The angle of this piece measured by the vision measuring system has a 95% confidence interval of 60.14 deg ± 0.09 deg based on five measurements of the same piece.

Though standard parameters can be used in zone 1, it is interesting to look at the influence of the power on the surface quality of the structure. Therefore, different samples are made with each time a different power of the first zone of the inclined structure. Figure 16 shows microscope images of these pieces.

From this figure, it is clear that power affects surface quality. Lower powers result in smoother surfaces whereas larger powers lead to less smooth downfacing surfaces.

Inclined angle of 45 deg. A structure with an inclination angle of 45 deg can also be produced with a power of 300 W (Fig. 18). The 95% confidence interval of the angle is 45.07 deg ± 0.48 deg based on five measurements of this inclined structure.

In analogy to the 60 deg. inclination angle, the influence of the power used in the first zone on the surface quality is investigated.

Figure 17 gives an overview of the microscope images. First of all, these surfaces are much less smooth than the surfaces that have an inclined angle of 60 deg. This confirms the expectations since this downfacing structure is a little more extreme. This rough surface also explains the larger confidence interval of the measured angle compared to the 60 deg. angle. Further, the differences in surface quality for different powers are less significant for this angle.

Inclined angle of 30 deg. An inclined structure of 30 deg cannot be produced by using only high powers. For this case, the strategy of Table 4 is used.

Figure 18(*c*) displays this structure. The microscope image is showed in Fig. 19. The surface of this piece is very rough.

The angle of this inclined structure is again measured by the vision measuring system. The 95% confidence interval based on five measurements is 31.44 deg ± 0.68 deg. The angle is clearly

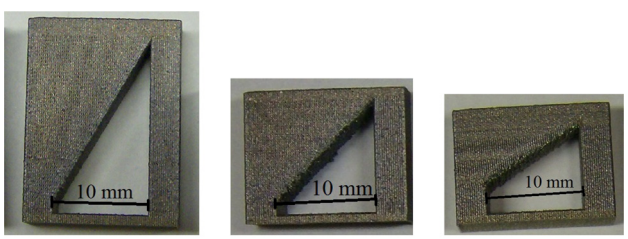

Fig. 19 Parts produced with inclined structures. (*a*) 60 deg, (*b*) 45 deg, and (*c*) 30 deg.

too large. This indicates that there is warp present due to thermal stresses. During the production of each layer, the end of the piece curls up a little further. Because of the limited size of the inclined structure, the warp did not cause problems during production. When the downfacing length increases, problems concerning the deposition unit are to be expected. (The curled up part blocks the deposition unit when placing a new layer of powder.)

4 Conclusion

In this research, scan strategies are optimized for AlSi10Mg.

First of all, the strategy to obtain high densities for upfacing structures is investigated. The combination of a power of 300 W and scan speed of 1400 mm/s results in relative densities of $99,3\% \pm 0,2\%$ (95% confidence interval).

Subsequently, scan strategy for downfacing structures are obtained. The scan pattern used is based on a scan pattern developed in Ref. [5]. Scan parameters are obtained based on simulations of a thermal model and on experimental tests. Simulations of a downfacing scanning situation using different parameters are compared to a simulation of a normal scanning situation. A downfacing power of 60 W results in similar melt pool dimensions compared to the normal scanning situation. Experimental tests show that no powder is melted when laser powers are too low. On the other hand, when laser powers are too high, lumps are formed.

Table 3 summarizes the scan strategy for downfacing structures.

Larger downfacing areas can be produced by using the parameter set of Table 3, but there are limitations. Long downfacing structures need extra supports on both sides to provide mechanical resistance and extra heat transport channels.

Finally, inclined structures are examined. When the angle between the inclined downfacing surface and a horizontal line is large enough, high powers can be used. Though, these high powers can be negative for surface quality. The research shows that low powers give better surface quality for an inclination angle of 60 deg.

For small angles, an adapted scan strategy is needed to prevent warp of the structure. Results show that even with this adapted strategy, some warp is present due to thermal stresses.

Acknowledgment

The research leading to these results has received funding from the European Union's Seventh Framework Programme (FP7/2007-2013) under Grant Agreement No. 314055.

References

[1] Edwards, P., O'Connor, A., and Ramulu, M., 2013, "Electron Beam Additive Manufacturing of Titanium Components: Properties and Performance," ASME J. Manuf. Sci. Eng., **135**(6), p. 061016.

[2] Mahamood, R., Akinlabi, E., Shukla, M., and Pityana, S., 2013, "Characterizing the Effect of Laser Power Density on Microstructure, Microhardness, and Surface Finish of Laser Deposited Titanium Alloys," ASME J. Manuf. Sci. Eng., **135**(6), p. 064502.

[3] Kempen, K., Thijs, L., Yasa, E., Badrossamay, M., Verheecke, W., and Kruth, J.-P., 2011, "Process Optimization and Microstructural Analysis for Selective Laser Melting of AlSi10Mg," Solid Freeform Fabrication Symposium, **22**(2011), pp. 484–495.

[4] Kempen, K., Thijs, L., Van Humbeeck, J., and Kruth, J.-P., 2012, "Mechanical Properties of AlSi10Mg Produced by Selective Laser Melting," Phys. Procedia, **39**, pp. 439–446.

[5] Clijsters, S., Craeghs, T., and Kruth, J.-P., 2012, "A Priori Parameter Adjustment for SLM Process Optimization," *Innovative Developments in Virtual and Physical Prototyping*, Taylor & Francis Group, New York, pp. 553–560.

[6] Wang, D., Yang, Y., Yi, Z., and Su, X., 2012, "Research on the Fabricating Quality Optimization of the Overhanging Surface in SLM Process," Int. J. Adv. Manuf. Technol. **65**(9–12), pp. 1471–1484.

[7] Mumtaz, K. A., Erasenthiran, P., and Hopkinson, N., 2008, "High Density Selective Laser Melting of Waspaloy®," J. Mater. Process. Technol., **195**(1–3), pp. 77–87.

[8] Buchbinder, D., Schleifenbaum, H., Heidrich, S., Meiners, W., and Bültmann, J., 2011, "High Power Selective Laser Melting (HP SLM) of Aluminum Parts," Phys. Procedia, **12**(2011), pp. 271–278.

[9] Vrancken, B., Thijs, L., Kruth, J.-P., and Van Humbeeck, J., 2012, "Heat Treatment of Ti6Al4V Produced by Selective Laser Melting: Microstructure and Mechanical Properties," J. Alloys Compd., **541**, pp. 177–185.

[10] Verhaeghe, F., Craeghs, T., Heulens, J., and Pandelaers, L., 2009, "A Pragmatic Model for Selective Laser Melting With Evaporation," Acta Mater. **57**(20), pp. 6006–6012.

[11] Mitutoyo American Corporation, 2013, http://ecatalog.mitutoyo.com/Vision-Measuring-Systems-C102.aspx

[12] Paul, R., Anand, S., and Gerner, F., 2014, "Effect of Thermal Deformation on Part Errors in Metal Powder Based Additive Manufacturing Processes," ASME J. Manuf. Sci. Eng., **136**(3), p. 031009.